Journal of the Korean Physical Society, Vol. 70, No. 6, March 2017, pp. 598∼605

Electrohydrodynamic Spinning of Random-Textured Silver Webs for Electrodes Embedded in Flexible Organic Solar Cells

Dai Geon Yoon
Micro/Nano Process Research Group, Korea Institute of Industrial Technology, Ansan 15588, Korea

Byung Doo Chin*
Department of Polymer Science and Engineering, Dankook University, Yongin 16890, Korea

Robert Bail
Department of Creative Convergent Manufacturing Engineering (CCME), Dankook University, Yongin 16890, Korea

(Received 24 January 2017, in final form 15 February 2017)

A convenient process for fabricating a transparent conducting electrode on a flexible substrate is essential for numerous low-cost optoelectronic devices, including organic solar cells (OSCs), touch sensors, and free-form lighting applications. Solution-processed metal-nanowire arrays are attractive due to their low sheet resistance and optical clarity. However, the limited conductance at wire junctions and the rough surface topology still need improvement. Here, we present a facile process of electrohydrodynamic spinning using a silver (Ag) - polymer composite paste with high viscosity. Unlike the metal-nanofiber web formed by conventional electrospinning, a relatively thick, but still invisible-to-naked eye, Ag-web random pattern was formed on a glass substrate. The process parameters such as the nozzle diameter, voltage, flow rate, standoff height, and nozzle-scanning speed, were systematically engineered. The formed random texture Ag webs were embedded in a flexible substrate by in-situ photo-polymerization, release from the glass substrate, and post-annealing. OSCs with a donor-acceptor polymeric heterojunction photoactive layer were prepared on the Ag-web-embedded flexible films with various Ag-web densities. The short-circuit current and the power conversion efficiency of an OSC with a Ag-web-embedded electrode were not as high as those of the control sample with an indium-tin-oxide electrode. However, the Ag-web textures embedded in the OSC served well as electrodes when bent (6-mm radius), showing a power conversion efficiency of 2.06% (2.72% for the flat OSC), and the electrical stability of the Ag-web-textured patterns was maintained for up to 1,000 cycles of bending.

PACS numbers: 73.50.Pz, 47.65.-d
Keywords: Organic solar cell, Electrospinning, Silver web, Embedded film, Flexible substrate
DOI: 10.3938/jkps.70.598

I. INTRODUCTION

A simple and low-cost process for the fabrication of a transparent electrode attracts significant attention for successful development of various flexible and lightweight thin-film devices, such as organic solar cells (OSCs), organic light emitting diodes (OLEDs) for lighting, transistors, sensors, and organic-biological devices. Application of a solution process or printing technology to the conductive track or electrode is advantageous for the formation of a transparent electrode, especially in terms of the economics of fabrication. Printed metal-ink-based electrodes [1–3], metal nanowires [4–7], and electro-sprayed sub-micron metallic nanofibers [8–10] are typical examples. Compared with the expensive vacuum deposition, these processes can provide a method for direct deposition of functional conductors on a substrate with a homogeneous, non-uniform, or a patterned surface.

Among the electrode materials, metallic nanowires are advantageous because they feature a synergistic combination of electrical and optical properties. However, several drawbacks, such as rough surfaces, poor adhesion to substrates, and instabilities against oxidation and moisture, still exist. Generally, the surface roughness of silver nanowire (AgNW) arrays on a flat substrate is large due to the spontaneous random arrangement of the AgNW networks. In this case, the stability of the device cannot be achieved, causing short circuit and failure. Several methods to overcome these phenomena have been reported, for example, embedding AgNW-network elec-

*E-mail: bdchin@dankook.ac.kr; Fax: +82-31-8021-7218

trodes in a polymer matrix or in an organic-inorganic hybrid film [11–13]. As an alternative, a metal grid-based electrode is also promising in terms of its simple and fast printable processes while the formation of a narrow and invisible grid for improved transparency requires lithography or imprinting. This increases cost and complicates the required experimental stages [14,15].

With the use of the electrohydrodynamic (EHD) jet process, metallic grids with line widths of $1 \sim 10$ μm can be fabricated using a simple procedure. The characteristic feature of this deposition technique is the pulling of liquids from a nozzle by an electric field. This initiates flow-induced elongation and break-up of ink droplets, whose sizes are typically smaller than the diameter of the nozzle [16, 17]. Accumulated ions in the inks near the meniscus of the nozzle experience Coulombic repulsion, which deforms the meniscus into a conical shape [18]. Such a "Tylor cone" formation is based on a simple mechanism, but phenomenological results show a quite complicated pattern formation, where the pattern size and shape depend on the ink viscosity, surface tension and conductivity, as well as on thermal factors. For example, the ink may immediately evaporate during the process when the substrate is heated. When the electric field strength is increased, the gravitational movement of jetting (dripping and bulk jet flow) changes to cone-jet mode (a stable condition for fine-pattern jet printing), followed by complicated instabilities, such as multi-jet features [19]. When the nozzle's inner diameter is in the range of 0.5 to 30 μm, the distance from the nozzle to the grounded substrate is small (~ 100 μm), and the electric field is relatively low, high resolution dots and line patterns with sizes in the range from 200 nm to 10 μm can be formed [2, 20]. However, when the distance between the nozzle's tip and the substrate is increased further, the jetting patterns are not straight (vertical), and random-texture patterns are generated. Although such random textures (webs) lack accurate alignment and positioning, the fast and continuous formation of metallic fibers produces much longer wires compared to AgNW. Thus, the EHD process should be useful applications in fabricating transparent electrode cores for flexible, thin film solar cells and lighting devices [21].

Herein, we report the insights gained from our investigation of modified EHD jet conditions for a formation of Ag line grid wire at a 300-μm standoff height between the nozzle and the grounded substrates. The results show that electrohydrodynamic spinning of silver webs (at a 4-mm height) is a fast and simple process for the manufacture of flexible wire-composite substrates. For a strong electric field and a moderate height, a web of fine Ag fibers was drawn from a source of viscous ink (Fig 1(a)). The web density was controlled by adjusting the deposition time and the air gap between the deposited fiber strands. These random-textured webs of silver fibers were embedded in composite polymeric films via a simple transfer and peel-off process, and the resulting structure could be utilized as an electrode-containing flexible substrate with an $\sim 80\%$ transparency and an ~ 1.2 Ω/sq resistivity. The electrical properties of the embedded Ag web-containing films were stable even after repeated bendings, and the properties of the organic solar cell were compared with those of indium-tin-oxide based control devices.

II. EXPERIMENTS

1. Fabrication of a Random-Textured Silver Web and an Electrode-Embedded Film

An EHD jet printer (*NT-professional, Enjet Corp., Korea*) was used for the electrospinning process, a schematic diagram of which is shown in Fig. 1(a). A stainless-steel nozzle (5 mm length) with an inner diameter of 100 μm was mounted on the printer head. The jetting conditions were as follows: The flow rate of ink from a syringe through a teflon tube to the nozzle tip was about 130 nL/min. The printing speed (*i.e.* scanning moves of the nozzle) was set to 100 mm/s with an acceleration of 1000 mm/s^2, and the applied voltage was 1.5 kV.

A silver nano-particle ink (*Paru Corp., Korea*) and a customized Ag paste ink [20] (*Enjet Corp., Korea*) were blended for 10 h by using a homogenizer and a vortex mixer to prevent phase separation between the silver nano-particles and the polymer binder in the customized paste. This yielded a silver ink with high viscosity suitable for electrospinning at a moderate standoff height under a strong electric field to produce a random-textured silver web pattern on a non-conducting substrate. The surface tension, density and viscosity of the Ag ink were 52.1 dyne·cm^{-1}, 3.3 g·cm^{-3} and 50,000 cPs, respectively. A continuous cone-jet line from the nozzle started to be extracted at a small standoff height (300 μm) while the electrospinning mode appeared under the same electric field but at a larger standoff height (4 mm), as shown in Fig. 1(a). After completion of the jetting process, the random-textured silver web sample formed on the glass substrate was sintered for 30 min on a hot-plate at 200 °C as a post treatment.

The web-embedded films were fabricated by coating the Ag-web electrode with two liquid, photopolymerizable monomers, ethoxylated bisphenol-A-dimetharcylate and tert-butylacrylate (both: *Sigma Aldrich, Korea*), using a blade coater on the random-textured web/glass substrates with various texture web densities as illustrated in Fig. 1(b). To achieve the formation of a 100-μm-thin film, ethoxylated bisphenol-A-dimetharcylate to tert-butylacrylate ratios of 5:5, 6:4, 7:3, 8:2, 9:1, and 10:0 (wt%:wt%) were tested. These mixtures always included 2,2-dimethoxy-2-phenyl acetophenone (*Sigma-Aldrich, Korea*) as a photoinitiator (1 wt%). The samples were exposed to UV light for 420 s to achieve photopolymerization. Then, they were immediately placed

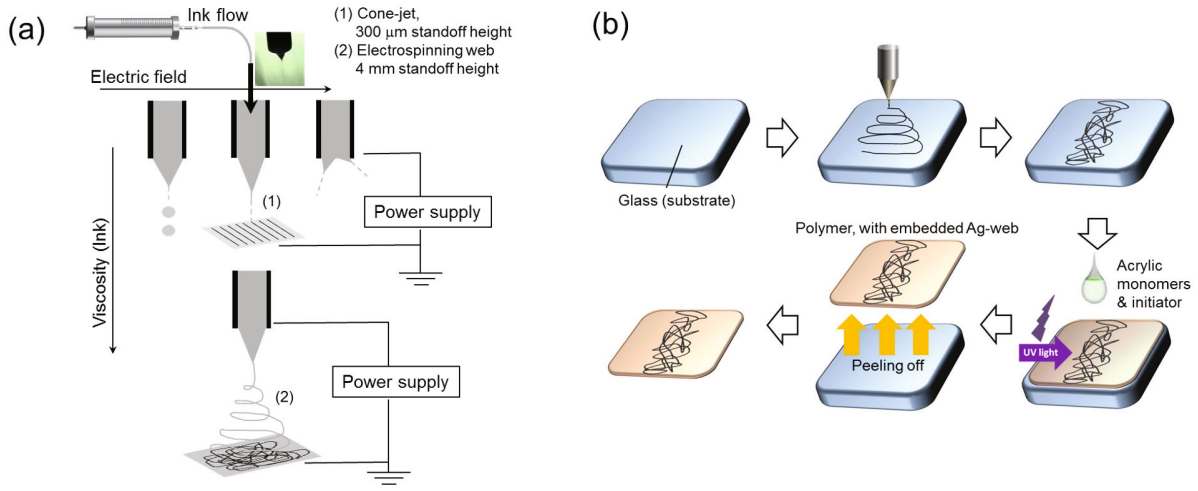

Fig. 1. (Color online) (a) Schematic illustration of the EHD process for different jetting conditions. (b) Diagram of the electrospun Ag-web random texture on a rigid substrate, followed by embedding into a polymer and a peel-off step.

in a refrigerator, where they remained for 120 s for a convenient releasing step so that it was possible to manually peel off the web-embedded polymer films from the glass substrate. Finally, the electrode-embedded films were cut into pieces sized 2.54 cm × 2.54 cm for the fabrication of OSC devices and sized 2.54 cm × 7.62 cm for the fabrication of samples used in the analysis of the electrical stability under bending.

The microscopic pattern profiles of the silver webs were analyzed with an interferometer (*NanoScan, Nanosystem Z corp., Korea*). The transmittance and the haze of the electrode-embedded polymer films were measured by UV-Vis spectrometry (*Lambda 950, PerkinElmer, Inc.*). The tensile stress vs. strain properties were measured using a universal testing machine (*Lloyd LR30K Plus, Ametek, Inc.*) to detect the break point under unidirectional elongation.

2. Fabrication and Characterization of Flexible OSCs

For the OSC devices, poly(3,4-ethylenedioxythiophene):poly(styrenesulfonate) [PEDOT:PSS, *Clevious-P, Heraeus Holding GmbH, Germany*] as a hole extracting layer with a roughness control function was spun-coated onto the silver web-embedded electrode at 3000 rpm for 30 s, which was followed by a baking process at 150 °C for 10 min. A blend of poly[(4,8-bis-(2-ethylhexyloxy)-benzo(1,2-b:4,5-b')dithiophene)-2, 6-diyl-alt-(4-(2-ethyl-hexanoyl)-thieno[3,4-b]thiophene-)-2-6-diyl] (PBDTTT-C, *SMI- P9001, Solamer Corp., China*) and [6,6]-phenyl-C_{71}-butyric acid methyl ester ($PC_{71}BM$, *Nano-c-PCBM-SF, Nano-C Corp., US*) was used as the photo-active layer, with PBDTTT-C:$PC_{71}BM$ 1:1.5 (wt%:wt%) in chlorobenzene. The photoactive material solution was spun-coated at 4000 rpm for 30 s and then annealed at 150 °C for 30 min under nitrogen. Finally, lithium fluoride (LiF; 0.5 nm) and aluminum (Al; 100 nm) were deposited using a thermal evaporation process. The layered device structure was substrate/embedded random-textured Ag-webs/PEDOT:PSS (40 nm)/PBDTTT-C:$PC_{71}BM$ (150 nm)/LiF (0.3 nm)/Al (100 nm). The I-V characteristics of the OSCs in the dark and under illumination (100 mW/cm^2) were measured with a Keithley 2400 source-measurement unit equipped with solar source (SUN200, ABET Technologies, Inc., US) at AM 1.5, and the values of the short-circuit current (J_{sc}), the open-circuit voltage (V_{oc}), the power conversion efficiency (PCE), and the fill factor (FF) were extracted.

III. RESULTS AND DISCUSSION

Microscopic images of the random textured silver webs indicated line diameters for the fabricated strands of approximately 5 to 10 μm, as shown in Fig. 2(a). These linewidths are very similar to those of the Ag-grid lines formed using EHD jet grid printing in cone-jet mode [Fig. 1(a)]. Parameters, such as the flow rate of the ink injector (130 nL/min), the pressure drop of the nozzle, and the applied voltage V_0 (1.5 kV), are identical for EHD jetting of straight lines [20] and for the electrospinning in this work. However, the ink viscosity (about × 10 higher for efficient electrospinning of Ag paste ink) and the standoff height (4 mm for spinning web formation), where the oriented Ag-polymer composite fibers were collected on the substrate with random-web texture, were different. Usually, the charged fibers leaving the nozzle tip are stacked on the collecting grids (electrode patterns) of the grounded substrates [21–23]. The jetted lines of silver-polymer ink on an insulator sub-

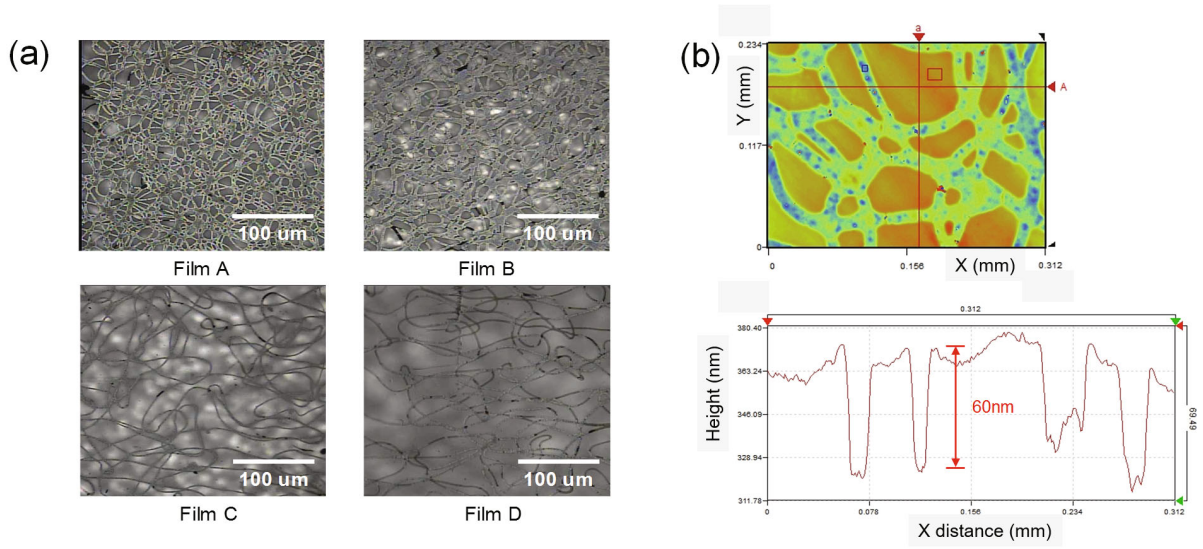

Fig. 2. (Color online) (a) Microscopic images of the random-textured Ag-web with different densities. Conditions were varied by the movement pattern of the nozzle following a line pattern of 50-, 100-, 200-, and 300-μm pitch. (b) 2D image data indicating the depth profile and roughness for Ag-webs embedded in the acrylic polymer substrate (Film C).

strate (here, pristine glass) are often less stable compared with those on a grounded conducting substrate. The formation of irregularly oriented webs is hence favored for relatively short distances between the nozzle's tip and the substrate. The high viscosity of the Ag-polymer paste ink, however, seems to be responsible for the generation of an electrospun web rather than sprayed droplets under an electric field. We prepared three samples of randomly oriented Ag webs with different average line-to-line pitches as illustrated in Fig. 2(a). The surface topology and the height of the Ag webs were further observed using interference microscopy [Fig. 2(b)]. The results showed a 60-nm-scale thickness and a width of less than 10 μm for the Ag web formed on a glass substrate. In case of film A, the nozzle moves under electrospun jetting conditions followed a line patterns with a 50-μm pitch while the scanning conditions for film B, C, and D produced a 100-, 200-, and 300-μm pitch, respectively (more spacious nozzle scanning position).

The two acrylic monomers, ethoxylated bisphenol-A-dimetharcylate and tert-butylacrylate, were mixed to improve the elasticity and the yield strength of the film, *i.e.* to optimize the design for flexible substrates in which a metallic web texture could be embedded. Table 1 shows the maximum elongation vs. mechanical load (strength, yielding point) of films for the tested monomer compositions. Although the ethoxylated bisphenol-A-dimetharcylate : tert-butylacrylate composition exhibited the highest yield strength at a ratio of 8:2 (wt%:wt%), the significant reduction in the elongation (9.7 mm to 6.8 mm) for this composition became a limiting factor. Therefore, the 7:3 composition of the monomers was selected for the fabrication of the Ag-web-embedded films and the OSC devices.

Table 1. Maximum elongation vs. mechanical load (strength; yielding point) of films with various composition of monomers.

Ethoxylated bisphenol -A-dimetharcylate: tert-butylacrylate (monomer ratio)	Max. elongation (mm)	Load for yielding point (N)
5:5	10.05	1.87
6:4	9.36	2.04
7:3	9.73	2.54
8:2	6.79	5.09
9:1	5.38	4.17
10:0	2.47	3.42

The transmittance data for the photo-polymerized and cured films with embedded Ag-web patterns are shown in Fig. 3. Compared to the optical transmittance of the control film (ITO/PET) of 78% at 550 nm, the Ag-web-embedded film with a proper line-to-line average pitch (film C) showed an 80% transparency. In the cases of films A and B with smaller line-to-line pitches, the transmittance was rather low compared to that of the control film. However, such optical properties can be further optimized by controlling the viscosity of the Ag-polymer ink paste, the base resin selection, and the density of the electro-spun web (fiber collecting time and moving speed of the stage), which should be simultaneously matched with the properly selected electrical-optical properties.

Although electrospun metallic fibers have several shortcomings, relatively long and continuous lines fill the entire surface of the substrate. As a result, the as-

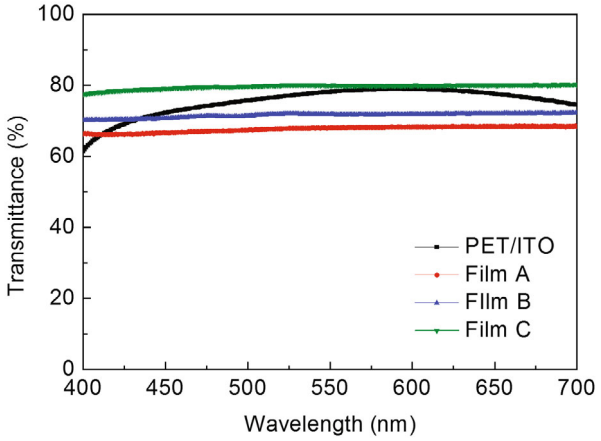

Fig. 3. (Color online) Transmittance data for Ag-web electrodes embedded in the film A, B, C, and PET/ITO (control).

pect ratio of the wires is significantly higher than that of most AgNW-network-based transparent electrodes [21, 22]. This may be the reason for the threshold percolation density of the Ag wire webs being significantly lower compared to those of AgNWs and carbon nanotubes (CNTs) [21,24]. Furthermore, the Ag-fiber-textured web fabricated by spectrospinning can provide a low junction resistivity due to electric-field-induced Joule heating and welding, especially under strong electric fields [25]. A free-standing metallic nanotrough network [26], formed by polymer nanofiber electrospinning, successive metal coating (deposition), and transfer to a selective substrate, showed remarkably higher electrical conductivity and transparency, but its excellence should be determined by the core-shell nature of nanoscale polymer-metal web and the complicated procedure. Also, in terms of the selection of the metal, an electrospun copper web generally exhibits the lowest resistivity whereas copper nanofibers formed from a metallic precursor/polymer composite source requires heating to 500 °C to remove the polymer stabilizer and a corresponding reduction step to convert CuO to Cu [21]. In this work, the silver wire electrospun from the viscous Ag nanoparticle-polymer paste ink produced a metallic web with dimensions larger than conventional AgNW or metal-polymer core-shell nanofiber webs. The wire diameter is still less than 10 μm, and the wire was barely visible to the naked eye [20]. Moreover, the stability of the metallic web may be better than of other nano-web composites, and the Ag-web can be prepared at a low sintering temperature.

We fabricated flexible OSCs by using the Ag-web-embedded polymer substrates. Figure 4(a) shows the current density-bias voltage (J-V) data for the OSCs (acrylate copolymer with embedded Ag web/PEDOT:PSS/PBDTTT-C:$PC_{71}BM$/LiF/Al) illuminated at 100 mW cm^{-2} (AM 1.5 G). For PET/ITO-based control device, the photovoltaic behavior shows a short-circuit current (J_{sc}) of 12.5 mA/cm^2, an open-circuit voltage (V_{oc}) of 0.63 V, and a fill factor (FF) of 0.48 (3.81% PCE; see Table 2), which are relatively low compared to those previously reported for glass substrates [27]. Under dark and illuminated conditions, the I-V characteristics of the OSCs fabricated on the various Ag-web-embedded films were determined. The OSC with film C (200-μm nozzle pitch) exhibited a J_{sc} of 9.27 mA/cm^2, a V_{oc} of 0.63 V, a FF of 47%, and a PCE of 2.72%. The lower J_{sc} and PCE values for the OSCs with smaller web pitches (higher web densities for films A and B), as seen in Table 2, can be explained by the reduced transmittances of these films [Fig. 3]. Furthermore, lower PCE and J_{sc} values for the device with film C (transmittance comparable to PET/ITO) may have originated from the higher reflection at the Ag-web-embedded film (approximately twice the value at PET/ITO), which should be further controlled to enhance the performance of the OSCs.

Table 2. Short-circuit current (J_{sc}), open-circuit voltage (V_{oc}), fill factor (FF), and power conversion efficiency (PCE) of OSCs for the control (PET/ITO) and various Ag-web-embedded substrates.

	ITO /PET	Film A	Film B	Film C	Film C, bent (6 mm curvature)
J_{sc} (mA/cm^2)	12.50	8.38	7.22	9.27	9.07
V_{oc} (V)	0.63	0.64	0.62	0.63	0.63
FF	0.48	0.48	0.47	0.47	0.36
PCE (%)	3.81	2.53	2.14	2.72	2.06

In spite of their lower performances as photovoltaic devices (J_{sc} and PCE), OSCs with embedded Ag-web electrodes are still advantageous in terms of operation under a curved geometry (6-mm bending radius), as seen in Fig. 4(b). Under bending, the OSC with film C exhibited a J_{sc} of 9.07mA/cm^2, a V_{oc} of 0.63 V, a FF of 0.36, and a PCE of 2.06%, which are somewhat lower than those of the flat devices, especially the fill factor. However, the OSC with PET/ITO was not operable at all when measured in the bended state.

The electrical properties of flexible and transparent electrode substrates were evaluated for a range of different bending radii and cycles, as seen in Figs. 5(a) and 5(b). Initially, the Ag-web-embedded substrates had resistances of less than 1 Ohm/cm while the resistance of ITO on PET was about 30 Ohm/cm (measured by using a 10 mm-spacing 2-probe). For comparison, the value of the sheet resistance for this PET/ITO was about 35 Ohm/sq. For ITO (possibly amorphous) on a polymer substrate, the crack density increased dramatically at increased bending momentum beyond a certain critical point of deformation, which explains the significant increase in the relative resistance of ITO/PET at smaller bending radii [28,29]. At a 6-mm bending radius, cracks seem to have already been formed at ITO/PET [Fig. 5(a)], whereas at a 10-mm bending radius, all films (A,

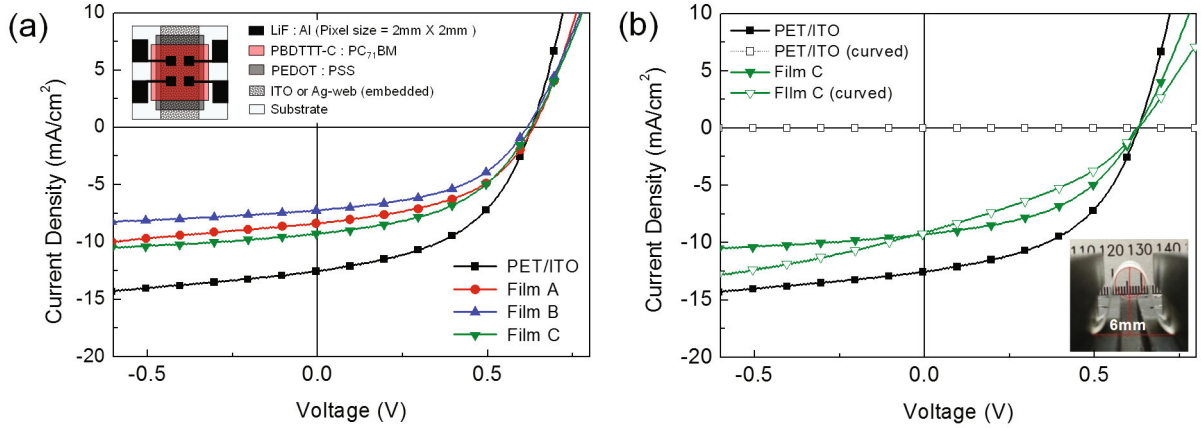

Fig. 4. (Color online) (a) Current density vs. bias voltage for OSC devices fabricated using various Ag-web transparent electrodes embedded in films and PET/ITO, (a) under flat condition and (b) in bent state (6-mm radius).

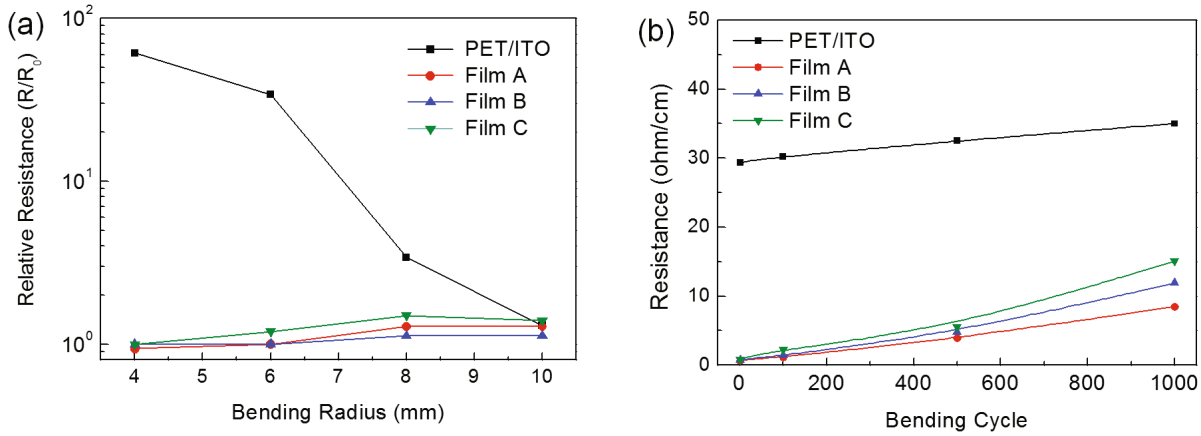

Fig. 5. (Color online) Electrical properties of bent Ag-web-embedded substrates: (a) bending radius vs. relative resistance and (b) bending cycle vs. resistance at 6-mm radius of curvature.

B, C and ITO/PET) revealed similar values for the relative resistance. This crack-induced deformation, already high at the initial stage of 6-mm bending of ITO/PET, may not become more significant for repeated bending up to 1000 cycles. The data shown in Fig. 5(b) (6-mm bending, 0 to 1000 cycles) indicate a gradual increase in the resistivity in the range of 30 $\sim$ 35 Ohm/cm for ITO/PET. Unlike the PET/ITO sample, we should note that the sheet resistance (Ohm/sq) for films A, B, and C cannot be simply defined as a flat layer because the upper layer of a textile-like web and its thickness are not uniform for the entire thickness of a sample.

Although the resistivity of the ITO/PET film underwent a significant increase for bending radii less than 8 mm [Fig. 5(a)], the values of the relative resistance R/R_0 (before/after bending) for the Ag-web-embedded films remained negligible for curvatures of 10 to 4 mm radius. For electrospun Ag-webs embedded in a polymer matrix film, a continuous buckling of the Ag web is believed to cause a non-recoverable deformation of the metallic wires with increasing numbers of deformation cycles. Typically, metallic wires are more stable than ITO thin films against extensive compression/tension at smaller bending radii. However, the accumulation of stress in metallic wires due to repeated bending might cause a continuous, gradual increase in the resistivity [Fig. 5(b)]. This results in a relatively "steep" resistivity-deformation time plot, even though the resistance remains under 15 Ohm/cm for Ag-embedded webs in polymer films. By contrast, the flexible ITO substrates were unable to show such low value for a 6-mm bending radius [Fig. 5(b)].

For a further evaluation of the optical properties for Ag-web-embedded acrylic films, the transmittance (direct and indirect) and the haze were measured (Table 3). As defined by ASTM D1003, haze is the percentage of light passing through that deviates from the incident beam by an angle greater than 2.5° on average (diffuse transmittance due to wide-angle scattering). Therefore, the total transmittance and the diffuse transmittance

Table 3. Optical properties of electrode/substrates: transmittance factors and haze (ASTM D1003).

	Film A	Film B	Film C	ITO/PET
T_{direct} (%)	57.19	67.15	79.23	72.81
T_{diffuse} (%)	1.38	1.26	1.22	3.33
T_{total} (%)	58.57	68.41	80.45	76.15
Haze* (%)	2.36	1.84	1.52	4.41

*Haze was characterized with the following equation: Haze $= 100\% \times \frac{T_{\text{diffuse}}}{T_{\text{total}}}$.

for wide-angle scattering were measured in order to estimate the haze. Interestingly, all samples showed low haze, which will be advantageous for applications of Ag-web-embedded films in a wide range of devices including light-emitting displays and free-form lighting. However, as reported elsewhere [30], the relatively large haze value of a AgNW-network electrode turned out to be even better for the achievement of OSCs with higher PCE. However, other applications, such as organic light-emitting diode-based illuminators, require the optimization of the metallic wire with high-index dielectrics for improved optical outcoupling efficiency.

Ag-web-embedded flexible substrates fabricated by using Ag paste ink and the electrospinning process have several drawbacks, such as lower transmittance (due to the relatively thick Ag-web compared to other polymer-metal composite nano-webs) under a sufficiently conductive condition (higher web density). However, their stability over an extended range of bending radii as well as a simple and low-temperature fabrication process is beneficial. Therefore, the Ag-web-embedded substrates developed in this study should have high potential for applications to various bendable and flexible OSCs and organic lighting devices.

IV. CONCLUSION

In this work, we have described the abnormal process of EHD jetting with viscous Ag-polymer paste ink, which accompanies the formation of an ultrafine meniscus when a 100-μm-diameter flow nozzle, a 4-mm standoff height between the nozzle and the insulator substrates, and a moderate electrical power (1.5 kV) are applied. The proper conditions for spiral injection (random network by electrospinning) originated from the formation of cone-jet mode in combination with lower-viscosity Ag inks at a 300-μm standoff height. Irregular patterns of Ag fiber networks were formed in the EHD spinning process, and those Ag wires were embedded in a soft acrylic polymeric film via the transfer and peel-off steps. As a result, a bendable OSC device with a 71% PCE, compared with an ITO-based control sample, was fabricated. The Ag-web-embedded film featured a PCE of 2.72% and was also operable in a bent state, showing a value of 2.06% PCE at a curvature of 6 mm. In addition, the random Ag-network electrodes embedded in a cured acrylic polymer maintained low resistivity after 1000 cycles of bending with a curvature of 4 mm.

ACKNOWLEDGMENTS

This work was supported by the research fund of Dankook University in 2014.

REFERENCES

[1] J. Perelaer, B. J. de Gans and U. S. Schubert, Adv. Mater. **18**, 2101 (2006).
[2] J-U. Park, M. Hardy, S. J. Kang, K. Barton, K. Adair, D. K. Mukhopadhyay, C. Y. Lee, M. S. Strano, A. G. Alleyne, J. G. Georgiadis, P. M. Ferreira and J. A. Rogers, Nat. Mater. **6**, 782 (2007).
[3] S. Jeong, K. Woo, D. Kim, S. Lim, J. S. Kim, H. Shin, Y. Xia and J. Moon, Adv. Funct. Mater. **18**, 679 (2008).
[4] Y. Sun, B. Mayers, T. Herricks and Y. Xia, Nano Lett. **3**, 955 (2003).
[5] U. Jeong, P. H. C. Camargo, Y. H. Lee and Y. Xia, J. Mater. Chem. **16**, 3893 (2006).
[6] L. Hu, H. Wu and Y. Cui, MRS Bulletin **36**, 760 (2011).
[7] E. C. Garnett, W. Cai, J. J. Cha, F. Mahmood, S. T. Connor, M. G. Christoforo, Y. Cui, M. D. McGehee and M. L. Brongersma, Nat. Mater. **11**, 241 (2012).
[8] H. Wu, D. Lin, R. Zhang and W. Pan, Chem. Mater. **19**, 1895 (2007).
[9] M. Bognitzki, M. Becker, M. Graeser, W. Massa, J. H. Wendorff, A. Schaper, D. Weber, A. Beyer, A. Golzhauser, A. Greiner, Adv. Mater. **18**, 2384 (2006).
[10] S. H. Choi, T. S. Hyun, H. J. Lee, S. Y. Jang, S. G. Oh and I-D. Kim, Electrochem. Solid-State Lett. **13**, A65 (2010).
[11] W. Gaynor, G. F. Burkhard, M.D. McGehee and P. Peumans, Adv. Mater. **23**, 2905 (2011).
[12] J. Jin, J. Lee, S. Jeong, S. Yang, J. Ko, H. Im, S. Baek, J-Y. Lee, B-S. Bae, Energy Environ. Sci. **6**, 1811 (2013).
[13] S. Nam, M. Song, D-H. Kim, B. Cho, H. M. Lee, J-D. Kwon, S-G. Park, K-S. Nam, Y. Jeong, S-H. Kwon, Y. C. Park, S-H. Jin, J-W. Kang, S. Jo and C. S. Kim, Sci. Rep. **4**, 4788 (2013).
[14] M. Kang, M. Kim, J. Kim and L. J. Guo, Adv. Mater. **20**, 4408 (2008).
[15] Y. Galagan, J. J. M. Rubingh, R. Andriessen, C. Fan, P. W. M. Blom, S. C. Veenstra and J. M. Kroon, Sol. Energy Mater. Sol. Cells **95**, 1339 (2011).
[16] J. U. Park, S. Lee, S. Unarunotai, Y. G. Sun, S. Dunham, T. Song, P. M. Ferreira, A. G. Alleyene, U. Paik and J. A. Rogers, Nano Lett. **10**, 584 (2010).
[17] M. S. Onses, E. Sutanto, P. M. Ferreira, A.G. Alleyne and J. A. Rogers, Small **11**, 4237 (2015).
[18] G. I. Taylor, Proc. R. Soc. London A **280**, 383 (1964).

[19] R. T. Collins, M. T. Harris and O. A. Basaran, J. Fluid Mech. **588**, 75 (2007).
[20] Y. Jang, J. Kim and D. Byun, J. Phys. D: Appl. Phys. **46**, 155103 (2013).
[21] H. Wu, L. Hu, M. W. Rowell, D. Kong, J. J. Cha, J. R. McDonough, J. Zhu, Y. Yang, M. D. McGehee and Y. Cui, Nano Lett. **10**, 4242 (2010).
[22] D. Li and Y. N. Xia, Adv. Mater. **16**, 1151 (2004).
[23] H. Wu, R. Zhang, X. X. Liu, D. D. Lin and W. Pan, Chem. Mater. **19**, 3506 (2007).
[24] J. Y. Lee, S. T. Connor, Y. Cui and P. Peumans, Nano Lett. **8**, 689 (2008).
[25] B. Seong, I. Chae, H. Lee, V. D. Nguyen and D. Byun, Phys. Chem. Chem. Phys. **17**, 7629 (2015).
[26] H. Wu, D. Kong, Z. Ruan, P-C. Hsu, S. Wang, Z. Yu, T. J. Carney, L. Hu, S. Fan and Y. Cui, Nat. Nanotech. **8**, 421 (2013).
[27] H-Y. Chen, J. Hou, S. Zhang, Y. Liang, G. Yang, Y. Yang, L. Yu, Y. Wu and G. Li, Nat. Photonics **3**, 649 (2009).
[28] S. K. Park, J. I. Han, D. G. Moon and W. K. Kim, Jpn. J. Appl. Phys. **42**, 623 (2003).
[29] D. R. Cairns, R. P. Witte II, D. K. Sparacin, S. M. Sachsman, D. C. Paine, G. P. Crawford and R. R. Newton, Appl. Phys. Lett. **76**, 1425 (2000).
[30] L. B. Hu, H. S. Kim, J. Y. Lee, P. Peumans and Y. Cui, ACS Nano **4**, 2955 (2010).